The Astrophysical Journal Letters, 944:L53 (9pp), 2023 February 20 https://doi.org/10.3847/2041-8213/acb651

A Potential Site for Wide-orbit Giant Planet Formation in the IM Lup Disk

Arthur D. Bosman[1], Johan Appelgren[2], Edwin A. Bergin[1], Michiel Lambrechts[2,3], and Anders Johansen[2,3]
[1] Department of Astronomy, University of Michigan, 323 West Hall, 1085 S. University Avenue, Ann Arbor, MI 48109, USA; ebergin@umich.edu
[2] Lund Observatory, Department of Astronomy and Theoretical Physics, Lund University, Box 43, SE-22100 Lund, Sweden
[3] Center for Star and Planet Formation, GLOBE Institute, University of Copenhagen, Øster Voldgade 5-7, DK-1350 Copenhagen, Denmark
Received 2022 October 31; revised 2023 January 19; accepted 2023 January 25; published 2023 February 22

Abstract

The radial transport, or drift, of dust has taken a critical role in giant planet formation theory. However, it has been challenging to identify dust drift pileups in the hard-to-observe inner disk. We find that the IM Lup disk shows evidence that it has been shaped by an episode of dust drift. Using radiative transfer and dust dynamical modeling we study the radial and vertical dust distribution. We find that high dust drift rates exceeding 110 $M_{\oplus}$ Myr^{-1} are necessary to explain both the dust and CO observations. Furthermore, the bulk of the large dust present in the inner 20 au needs to be vertically extended, implying high turbulence ($\alpha_z \gtrsim 10^{-3}$) and small grains (0.2–1 mm). We suggest that this increased level of particle stirring is consistent with the inner dust-rich disk undergoing turbulence triggered by the vertical shear instability. The conditions in the IM Lup disk imply that giant planet formation through pebble accretion is only effective outside of 20 au. If such an early, high-turbulence inner region is a natural consequence of high dust drift rates, then this has major implications for understanding the formation regions of giant planets including Jupiter and Saturn.

Unified Astronomy Thesaurus concepts: Protoplanetary disks (1300); Exoplanet formation (492)

1. Introduction

The formation of giant planets, like Jupiter in our own solar system, has long been a challenge for planet formation models. The gas-dominated mass budget of these planets implies an early formation of the planet; that is, within 1–3 Myr of the formation of the host star while abundant gas is still present in the protoplanetary disk (e.g., Haisch et al. 2001). The main bottleneck in the creation of a giant planet is the formation of the core, which has to grow massive enough to start runaway gas accretion (e.g., Pollack et al. 1996). Traditional oligarchic models of giant planet core formation models have difficulties with reaching this critical mass within the timescale necessary for the accumulation of a massive atmosphere (see, e.g., Johansen & Bitsch 2019). This limits the formation of giant planets relatively close to the star (inner few astronomical units).

An alternative method of core formation, pebble accretion, in which a core grows by the rapid accretion of millimeter- to centimeter-sized solids (pebbles) has slowly been gaining traction (e.g., Johansen & Lambrechts 2017; Ormel 2017; Drazkowska et al. 2022). This method has the advantage that giant planet cores can be built quickly (<1 Myr) and at a far wider range of radii (Lambrechts & Johansen 2012; Bitsch et al. 2019; Johansen & Bitsch 2019). However, it requires that millimeter- to centimeter-sized solids (pebbles) be rapidly transported radially inward through the disk midplane, a process known as pebble drift (Weidenschilling 1977). This process has long been proposed to be present in protoplanetary disks, but little to no observational evidence is present. However, models of efficient drift generally result in a pileup of dust in the inner disk which should be observable (e.g., Birnstiel et al. 2012; Pinte & Laibe 2014).

The advent of the Atacama Large Millimeter/submillimeter Array (ALMA) has significantly changed the landscape of dust physics and planet formation. High-resolution observations are finding structures in many disks at large (>10 au) radii (Andrews et al. 2018; Huang et al. 2018) that are most likely planet induced. This implies that massive planets can form quickly at large radii (Zhang et al. 2018; Teague et al. 2019). However, other origins for the disk structures have been suggested (Hu et al. 2022; Rabago & Zhu 2021). Furthermore, ALMA has been able to confirm the existence of pebbles in a thin layer near the disk midplane (e.g., Pinte et al. 2016; Villenave et al. 2022). These observations lent strong credence to pebble accretion as a major planet formation pathway.

As aforementioned, direct evidence of strong pebble drift as a robust physical process that should take place in protoplanetary disks has so far been missing. It is suggested that the ratio between gas and dust disk size, if suitably large, $R_{\rm gas}/R_{\rm dust} > 3$, could be a signpost of drift. However, this is only seen in a small subset of disks (∼15%; e.g., Trapman et al. 2019), indicating that drift happens only in a small fraction of disks, or, more likely, that radial drift of dust can leave a remnant radially extended dust disk behind. Further evidence for radial drift can be found in the transport of ices on pebbles surfaces. When the pebbles drift from the cold outer disk to the warmer inner regions they bring with them an ice mantle. When these pebbles reach the warmer regions, species in the ice sublimate, enriching the gas (e.g., Cuzzi & Zahnle 2004). An enhancement in CO gas has been found around the temperature that CO should sublimate in the disk of HD 163296, which has been attributed to dust drift (Zhang et al. 2020). Finally, a relation has been found between the water emission coming from the innermost regions and the sizes of pebble disks, a possible proxy for pebble drift efficiency (Banzatti et al. 2020). While these papers all give evidence for drift happening, they do not give a quantitative pebble drift rate, and so can not comment on the effect of drift on planet formation.

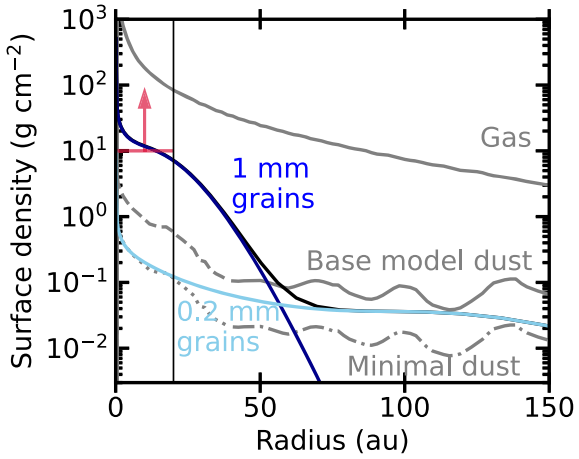

Figure 1. Surface densities of the gas and dust of IM Lup. The solid gray lines show the gas and dust from the model from Zhang et al. (2021), which is the baseline for our DALI models. The dashed–dotted gray line shows the minimal amount of dust required if purely 0.2 mm particles are responsible for the 1.3 mm dust emission. In the inner 40 au, the dust is optically thick and thus the derived surface density is uncertain. Dark and light blue lines show the predictions of our drift model for 1 mm, assuming a global gas-to-dust ratio of 100, and 0.2 mm grains, assuming a global gas-to-dust ratio of 1000, respectively (see Appendix B). Both models are taken at 0.6 Myr, the time at which the 1 mm grains have a large pileup in the inner 20 au. The dark red arrow shows the limit for 400 $M_\oplus$ within 20 au, as derived previously (Bosman et al. 2021). Our dust model predicts that we can create an inner-disk pileup with significant mass in the inner disk with 1 mm grains, while just 10% of the total dust mass in 0.2 mm grains leaves enough opacity in the outer disk to explain the continuum emission further out in the disk.

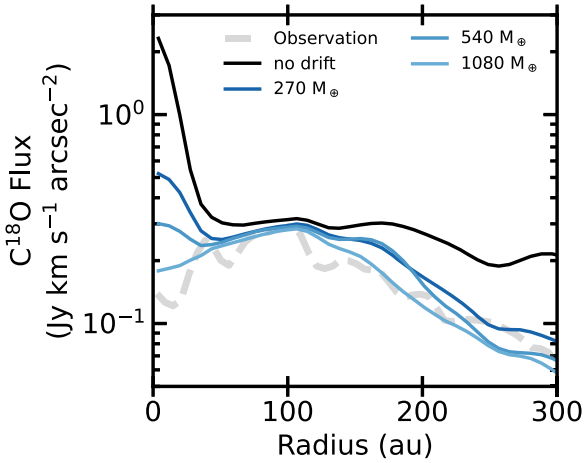

Figure 2. Comparison between the observed $C^{18}O$ radial profiles (Law et al. 2021; gray) and simulated observations. A model without drift is shown in black. Colored lines show models with an increased surface density in the inner disk due to drift. The 540 $M_\oplus$ model is the 1 mm drift model shown in Figure 1; the others are the same model scaled up or down a factor of 2 in surface density. An inner-disk mass of more than 540 $M_\oplus$ within 20 au is required to have an inner-disk depression.

Recent observations of the young (∼1 Myr) IM Lup disk have provided more direct evidence (Mawet et al. 2012; Cleeves et al. 2018; Bosman et al. 2021; Sierra et al. 2021). Analysis of the inner ∼20 au imply that this region contains a surface density of large dust that is 10–100 times higher than expected from an extrapolation of the outer disk. This is a smoking gun for efficient pebble drift, and would imply pebble drift rates >40 $M_\oplus$ Myr^{-1}. In Bosman et al. (2021) we showed that an inner-disk pileup is consistent with the CO isotopologue data. Here we take a deeper look at the total mass concentrated in the inner disk and the implication these observations have on planet formation inside 20 au.

2. Methods

To extract the physical conditions in the inner IM Lup disk, we combine a thermochemical model (Bruderer et al. 2012; Bruderer 2013) with a physical setup developed for IM Lup (Zhang et al. 2021). We then compare our observational findings with a disk evolution model that includes radial dust drift (Appelgren et al. 2020). From this model we simulate CO isotopologue observations that we compare to observations (Law et al. 2021). The base of the model is the gas and dust structure from Zhang et al. (2021). The full model setup is detailed in Appendix A and the surface densities used are shown in Figure 1. The model contains two dust components, small dust (0.005–1 μm), which follows the gas distribution, and a large dust component (0.005–1000 μm), which has a varying scale-height scaling.

The inner disk of IM Lup shows a flux depression in CO isotopologues (Figure 2, gray line; Law et al. 2021). In particular, $C^{18}O$ stood out, as the wings of the $C^{18}O$ line profile showed that the flux from the inner 20 au was suppressed below the detection limit. A fit to the CO isotopologue emission with a decrease in the CO abundance required an excessively low CO abundance (Zhang et al. 2021) with the two $J = 2$–1 and $J = 1$–0 $C^{18}O$ lines predicting CO columns that are an order of magnitude apart. As such, in our model we assume a constant CO abundance, and instead use dust opacity to lower the inner-disk line flux. As discussed in Bosman et al. (2021), suppression of line emission requires the large dust grains to be significantly vertically extended, so that the line photons can be scattered and absorbed by the dust. Therefore, our models assume that the large dust is fully vertically extended, that is, the dust scale height is the same as the gas scale height within 30 au.

To get a physically motivated dust surface density, a dust evolution model tuned to the IM Lup disk is run for 1 Myr (see Appendix B for the full model setup). The resulting dust pileup is used as a physically motivated guide for the radial dust density structure of the inner disk. For the outer disk we use the observationally derived dust surface density (Zhang et al. 2021). We take this dust surface density as our base, no drift, dust model. These dust surface densities are not accurate in the inner optically thick regions of the disk. Here we replace the image derived dust surface density by the 1 mm grain drift model prediction (Appendix B). This model contains ∼540 $M_\oplus$ within the inner 20 au. We also use inner-disk dust surface densities where the surface density is scaled up and down by a factor of 2 to capture the uncertainties in the dust drift models.

While we use the dust and gas surface density of the Zhang et al. (2021) model in our models, we do not expect perfect agreement between our model and the data that was fitted by the Zhang et al. (2021) model. This is due to the vertically extended dust that we include in the inner 30 au in all of our models. This strongly changes the radiation field in the entirety of the disk. This will affect the dust temperature, and thus the continuum flux, as well as strongly affect the gas temperature and thus the line flux of ^{13}CO as well as ^{18}CO at larger radii. A mismatch in absolute flux between the model and the observations is thus expected. This should not impact the masses derived for the inner disk.

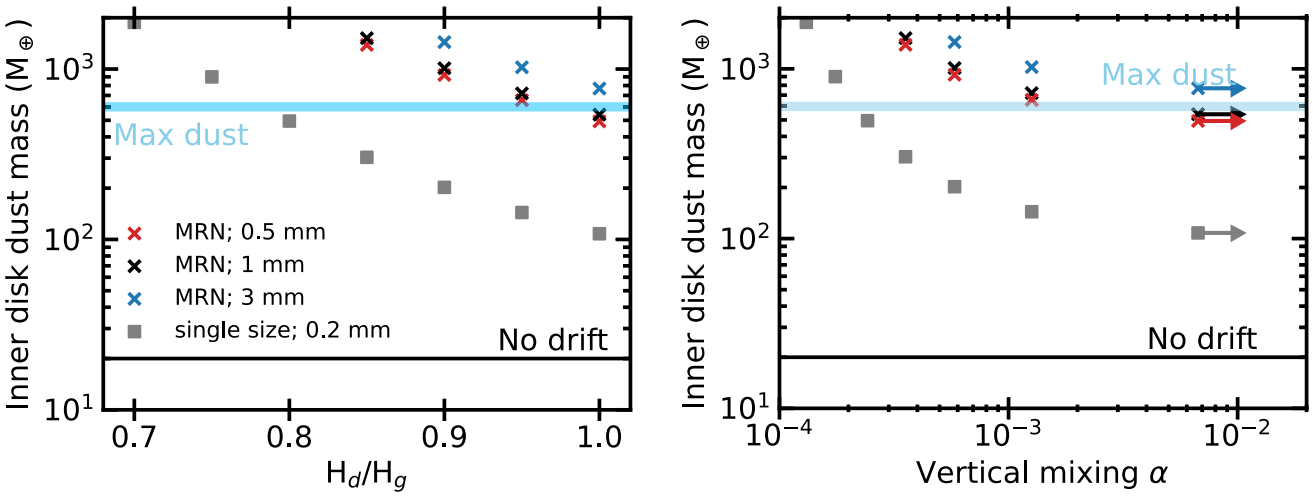

Figure 3. Left: required dust mass to suppress the $C^{18}O$ in the inner 20 au of IM Lup as a function of the dust scale height. Crosses assume a dust size distribution from 0.005 μm to the listed size with a power-law slope of −3.5. Squares assume all the dust is a single size, 0.2 mm, which yields the highest opacity at 1.3 mm. Blue vertical line shows the maximal total refractory mass in the IM Lup disk. Right: same as on the left, but the H_d/H_g converted into a vertical mixing α assuming the dust of 0.2 mm size is dominating the opacity and needs to be elevated to the listed H_d/H_g (Johansen et al. 2014). Points with arrows take the mass for $H_d/H_g = 1$, and show the α for $H_d/H_g = 0.99$, as an infinite α is required for $H_d/H_g = 1$. A high $\alpha > 0.001$ is required when a full dust size distribution is assumed. Only under the assumption that the dust is 0.2 mm sized will $\alpha < 10^{-3}$ solutions be possible.

3. Results

Figure 2 shows a comparison between the $C^{18}O$ model simulation and observations. The base model, without any drift, exhibits a centrally peaked CO emission profile inside 20 au. However, the data requires a strong dip in this region. Such a dip in the inner ∼20 au is only present in the simulation if the inner-disk dust surface density is at least 10 g cm^{-2}, or a gas-to-dust ratio <10. At that point the dust $\tau = 1$ at 1.3 mm sits around or above the $\tau = 1$ surface for the $C^{18}O$ $J = 2$–1 line emission, allowing the dust to absorb the line photons.

This corresponds to a mass reservoir of at least 540 $M_\oplus$ within 20 au. The model with 1080 $M_\oplus$ shows behavior closer to that of the observations. The comparison between the model and observations for ^{13}CO also suggests that higher dust surface densities are required (details provided in Appendix A). However, for our further derivations we will use the lower limit of 540 $M_\oplus$.

The dust content in the inner disk expected from the gas surface density and a gas-to-dust ratio of 100, without the presence of any dust transport, is ∼20 $M_\oplus$. Therefore, most of the mass currently inferred in the inner disk had to be have been transported into the inner 20 au from the outer disk. With the current age of IM Lup of <1 Myr (Mawet et al. 2012), this would require a dust drift rate of >540 $M_\oplus$ Myr^{-1}.

3.1. Dust Mass in the Inner Disk

A dust size distribution with a higher opacity would require less mass, while a dust size distribution that is less vertically extended would require more mass. To explore this we calculate the dust mass required for dust distributions. For simplicity, we assume the vertical extent of the millimeter-opacity and mass-dominating large dust can be modeled with a single H_d/H_g. Our standard model uses the "large grain" dust opacity from Birnstiel et al. (2018). This assumes a dust size distribution between 0.005 μm and 1 mm, with a power-law size distribution with a slope of −3.5. Opacities were also calculated assuming the largest grains are 0.5 or 3 mm as well as under the extreme assumption when all dust is 0.2 mm in size. The latter assumption provides a strict lower limit, as 0.2 mm grains give the maximum extinction per unit dust mass at 1.3 mm. We also calculated the mass required if the dust was more vertically settled, by requiring the dust $\tau = 1$ surface at 1.3 mm to be at the same height as in our $H_d/H_g = 1$ model.

Figure 3 shows the required dust masses under these assumptions. These dust masses are compared to the maximal amount of dust that can be present in the full IM Lup disk. The gas mass in the IM Lup disk model is 0.2 $M_\odot$, about 20% of the stellar mass (Zhang et al. 2021). This is on the upper end of the mass the disk can have before it becomes dynamically unstable (Toomre 1964). Assuming a standard interstellar medium (ISM) gas-to-dust ratio of 100, which corresponds to about 600 $M_\oplus$ of refractories or ∼1000 $M_\oplus$ of total solids, assuming all H_2O and CO is frozen out. For grain size distributions that include grains larger than 5 mm or single-grain size populations smaller than 0.15 mm, the required mass to efficiently extinguish the CO emission is greater than the total available mass.

Figure 3 also shows that the large dust must be significantly lofted into the disk surface layers; in the optimal case of pure 0.2 mm grains, the dust scale height is >0.75 times the gas scale height. In the cases where there are larger grains in the inner disk, the many opacity-providing grains of ∼0.2 mm size need to be lofted to at least 90% of the gas scale height. Neither case is close to the expected thin midplane layer of grown dust that is seen in the outer regions of disks (e.g., Dullemond et al. 2018).

The extended vertical distribution of grains implies that the dust is being mixed up by some form of turbulence. We can derive a turbulent α_z from the particles' Stokes number (St) and the required H_d/H_g using

$$\frac{H_d}{H_g} = \sqrt{\frac{\alpha_z}{\mathrm{St} + \alpha_z}} \quad (1)$$

(Johansen et al. 2014). To get a strict lower limit on α, we take the Stokes number of the opacity-dominant 0.2 mm grains. This reveals that for the grain size distributions, high levels of α are required, $\alpha_z >> 10^{-3}$, to keep the inner-disk mass reservoir under the total available disk dust mass. In the

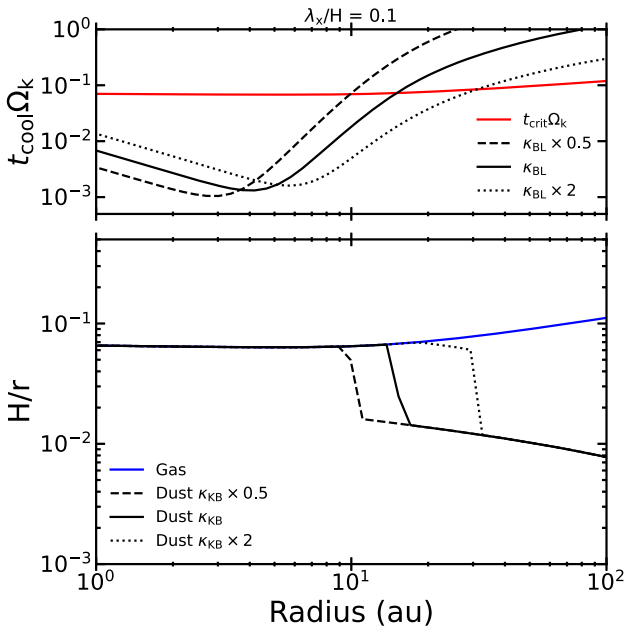

Figure 4. Top: the dimensionless cooling time $t_{\rm cool}\Omega_{\rm k}$, assuming a VSI wavelength mode of $\lambda/H = 0.1$. Below a critical cooling time (red), the disk cools quickly enough that the VSI can become active. The sensitivity of the VSI-active region on opacity ($\kappa_{\rm KB}$) is illustrated by increasing (dashed) or decreasing (dotted) the opacity by a factor of 2. Bottom: the effect of VSI turbulence in the inner disk on the scale height of millimeter-sized particles. The gas scale height is shown in blue, while the millimeter-sized dust scale height is shown in black for our nominal opacity. Also, here the sensitivity on the opacity is shown with dashed and dotted curves.

extreme case of all dust mass confined to 0.2 mm grains, α_z down to 2×10^{-4} is possible, but this scenario is highly unlikely. A grain distribution out to grains of 3 mm seem to be ruled out, on the condition that $\alpha_z \gg 10^{-2}$.

3.2. Turbulent Implications

The CO isotopologues imply that $\gg$100 $M_\oplus$ of dust is piled up within the inner 20 au of the disk. This requires significant dust drift rates $\gg$100 $M_\oplus$ Myr^{-1}. Our dust dynamical models show that enough dust can be transported into the inner disk if the dust sizes are around 1 mm. This particle size is consistent with the fragmentation limit in disks with low turbulent stirring, where the α is $\lesssim 10^{-3}$ (Birnstiel et al. 2010). Such a low degree of particle turbulence is consistent with dust observations of the outer parts of protoplanetary disks (Pinte et al. 2022). In the inner disk, however, the dust needs to be efficiently vertically distributed. This requires high levels of vertical turbulence ($\alpha_z > 10^{-3}$). The magento-rotational instability, and other (nonideal) MHD effects can stir up the dust particles (Riols & Lesur 2018; Yang et al. 2018); however, it is not clear why this would lead to such a strong discrepancy in particle scale heights, as seen in IM Lup.

It is thus more likely that there is another process that increases the vertical turbulence and elevates grains to the heights required by the observations. A prime candidate for driving large-scale vertical gas motions is the vertical shear instability (VSI; Urpin & Brandenburg 1998; Nelson et al. 2013). This instability is triggered when the stabilizing vertical buoyancy forces are overcome by vertical shear in the disk, which requires gas cooling timescales that are shorter than orbital timescales, $t_{\rm cool} \ll t_{\rm orbit}$ (Lin & Youdin 2015; Fukuhara et al. 2021).

Figure 4 shows the relation between the midplane cooling time and the critical cooling time for the VSI to operate in more detail. Here we use standard assumptions that follow Lin & Youdin (2015) and a VSI-unstable wavelength of $\lambda_x/H = 0.1$ (see Appendix C for details and a further parameter exploration). The requirement for sufficiently short cooling times is typically not met in the very outer, optically thin parts of the disks ($\gtrsim$50 au). However, the exact location of this outer boundary of the VSI-active region depends sensitively on the dust opacity, as $t_{\rm cool} \propto \kappa^{-1}$ (Lin & Youdin 2015). For our disk model we find that the VSI cooling criterion is satisfied out to 20 au, using nominal Rosseland mean dust opacities (Bell & Lin 1994). A factor of 2 change in opacity can lead to a factor 2 change in outer boundary radius.

Furthermore, Figure 4 shows the resulting particle scale height of millimeter-sized grains when using a conservative vertical turbulent stirring rate of $\alpha_z = 2.5 \times 10^{-3}$ in the VSI-prone region. This vertical stirring α_z is based on global numerical simulations of VSI-unstable disks (Flock et al. 2017). The vertical stirring by the VSI gas motions puffs up the pebble layer, such that millimeter-sized grains are elevated up to the gas scale height over nearly the entirety of the VSI-prone region. Outside this radius, we have here assumed lower vertical particle stirring, $\alpha_z = 1 \times 10^{-4}$, more in line with outer-disk nonideal MHD particle diffusion (Riols & Lesur 2018) and the observed low particle scale heights at wide orbits in other protoplanetary disks (Pinte et al. 2016; Villenave et al. 2022).

4. Discussion

4.1. Implications for Planet Formation

The observations of IM Lup imply a split between two regions of the disk: an inner region ($\lesssim$20 au) where dust is piled up and vertically extended distributed, and an outer disk ($\gtrsim$20 au) where dust is efficiently being transported in through radial drift (see Figure 5).

Efficient drift in the outer disk implies relatively high Stokes numbers (>0.01; Weidenschilling 1977; Birnstiel et al. 2010) and high St/α (e.g., Birnstiel et al. 2012), which should lead to well-settled grains (Johansen et al. 2014). The inner-disk dust pileup implies that at least 110 $M_\oplus$, and more likely $\gg$110 $M_\oplus$ has been transported from the outer disk into the inner 20 au within the 1 Myr age of the IM Lup disk (Mawet et al. 2012). This scenario is ideal for the formation of giant planet cores at larger (>20 au) radii (Bitsch et al. 2019; Johansen & Bitsch 2019).

In contrast, the high pebble scale heights, implying low St or high α, required to fit the observations will have an adverse effect on the efficiency of pebble accretion, quenching giant planet formation in the majority of the inner 20 au region (Lambrechts & Johansen 2014). The Stokes numbers for the dust in the inner disk must be small to impact the CO emission. For example, 1 mm particles at 20 au have a St $= 6 \times 10^{-4}$. This implies that, even with the large dust surface densities and high metallicity in the inner 20 au, the streaming instability might not be triggered (Carrera et al. 2015; Yang et al. 2017; Li & Youdin 2021).

If a stage like this is common for massive protoplanetary disks, it could explain the formation of planets at large radii

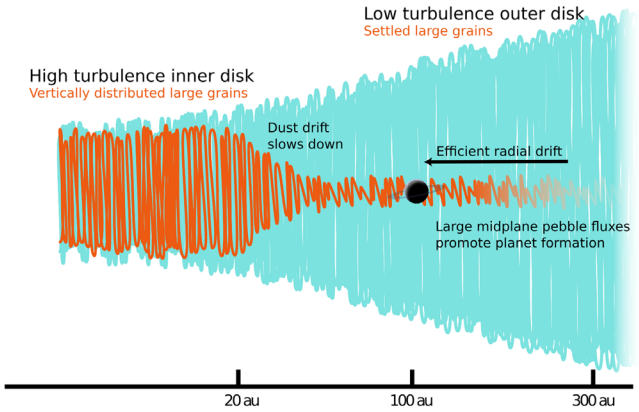

Figure 5. Schematic of the dust (orange) and gas (blue) distributions in the IM Lup disk. A planet image has been put in the approximate position of a proposed protoplanet around 100 au (Pinte et al. 2020; Verrios et al. 2022).

invoked to explain dust and gas structures in a variety of older protoplanetary disks (e.g., Zhang et al. 2018; Pinte et al. 2022). In fact, IM Lup is proposed to have a forming planet out at 117 au (e.g., Zhang et al. 2018). An inner disk with high turbulence and small pebbles as a result of strong pebble drift would also predict that giant planet formation due to pebble accretion is strongly suppressed in the inner disk.

Formation of giant planets this far out in the disk would have a massive impact on the composition of the material that they would accrete. In particular, the pebbles that are forming the core would bring in large amount of very volatile ices like CO, N_2, Ar, Kr, and Xe, which would be absent from the pebble ice in the warmer inner regions. Enhancements of these species have been observed in the atmosphere of Jupiter in the solar system, implying that Jupiter formed far from its current location and that the early solar system might have gone through a state similar to what we see IM Lup in now (Bosman et al. 2019; Öberg & Wordsworth 2019).

Interactions between (forming) planets and their natal disks is expected to cause significant migration of planets. Planets forming at large radii (>50 au) can end up very close to the star. Planets formed far out can thus be the progenitors of some or all of the giant planets on close orbits we see now. Efficient migration is also required to match the protoplanetary disk mass and size distribution with the observed giant exoplanet distribution (Mulders et al. 2021).

4.2. Alternative Scenarios

A drop in CO isotopologue flux can have other causes than the dust pileup proposed here. Zhang et al. (2021) modeled the CO flux with very low CO abundances in the inner disk. However, derivations from the $J = 2$–1 and $J = 1$–0 $C^{18}O$ lines disagree on the CO abundance by an order of magnitude. As both these lines come from the same isotopologue, this cannot be reconciled with any chemical explanation. However, if the dust is absorbing line emission then the wavelength-dependent opacity of the dust can naturally explain why between the 1.3 mm $J = 2$–1 and 3 mm $J = 1$–0 $C^{18}O$ that the lines are differently impacted. Radial profiles by Law et al. (2021) show, however, that all robustly detected lines across all observed species share the inner-disk depression. This is not naturally explained by a low CO abundance, but is expected from a puffed up inner-disk pileup.

A reduced gas surface density in the inner disk would be able to explain the decreased line flux. The clear drop in the $J = 2$–1 ^{13}CO line would then imply that this line becomes optically thin. At a conservative inner-disk CO abundance of 10^{-5} with regards to H_2, this implies a gas surface density <0.06 g cm^{-2}, or a gas surface density decrease of at least three orders of magnitude (e.g., Bosman et al. 2021). This is inconsistent with the high gas accretion rate $\sim 10^{-8}$ $M_\odot$ yr^{-1} measured for IM Lup (Alcalá et al. 2017). We therefore conclude that the inner-disk dust pileup is consistent with a larger range of observations than alternative scenarios.

4.3. Finding More Drift-heavy Disks

The leaves the question as to how common the formation of a dust pileup with vertically extended dust is. If it is the VSI that is triggered by strong dust drift and subsequent inner-disk pileup, the process might be universal to disks with large dust drift rates. To test this, however, one needs to find other disks in the same state as IM Lup. Analyzing the CO isotopologue emission in the inner disk would be a good way of determining inner-disk dust pileups. However, observations with the same sensitivity and resolution as those available for IM Lup are too time consuming to do for a large sample of disks. As such, some preselection is required.

In multiwavelength continuum observations, the inner disk looks different from the outer disk, with the inner disk having a flatter spectral slope than the outer disk. This could be caused by the dust pileup, increasing the optical depth, or the higher turbulence, changing the grain size distribution and thus the optical properties (Sierra et al. 2021). As such, this could be a marker of extreme drift.

Episodes of extreme drift are short-lived, constrained by the dust mass reservoir of the disk. As such, a search should be focused toward young disks, in particular those still embedded in their natal envelope, known as Class I disks. Observations probing the inner $\sim$30 au regions are rare, and a direct counterpart of the IM Lup data does not exist for any of these sources. However, Harsono et al. (2020) aimed to detect water vapor originating from the inner regions of these Class I sources. Contrary to expectations, water vapor was not detected. If the inner disks of these Class I objects are shaped by the same processes as IM Lup, then the abundant, lofted dust would suppress the water emission from the inner 20 au, similar to the suppression in the inner-disk $C^{18}O$ emission from IM Lup.

Finally, IM Lup stands out in another inner-disk tracer, its mid-IR spectrum. It is one of only a handful of sources that shows just CO_2 without the H_2O, HCN, and C_2H_2 that are commonly seen in the same part of the spectrum (Salyk et al. 2011; Bosman et al. 2017). This could be caused by drift, as well as abundant small grains in the surface of the inner disk and, as such, could be a signpost of a recent episode of drift and strong stirring in the inner disk. Strong drift is expected to enrich the inner disk with water, which is in turn expected to suppress the abundance of HCN and C_2H_2 and increase the abundance of CO_2. Abundant grains in the surface layers limit the region where mid-IR molecular lines can be generated. This leaves only the top low-density region of the disk above the layer of elevated optically thick dust. In this region the density is too low to excite any of the IR transitions collisionally. The 15 μm bending mode of CO_2 can still be excited by IR continuum photons and would thus still be

observable (Bosman et al. 2017). If this is indeed the case then the bending mode of water at 6.5 μm might also be visible in emission, even though the pure rotational lines at 12–30 μm are not observed as these transitions can also be directly excited by continuum photons (Bosman et al. 2022).

5. Conclusions

The IM Lup system poses an interesting case study for planet formation through pebble accretion. The inner 20 au shows a strong enhancement of large dust that requires a continuous or very recent (<1.0 Myr) massive pebble flux, with pebble drift rates significantly higher than 110 $M_\oplus$ Myr^{-1}. These conditions allow for the fast formation of giant planet cores. In the inner 20 au, however, the dust has to be vertically extended to impact the line emission. A vertically extended dust distribution is predicted to greatly slow down the formation of giant planet cores through pebble accretion. The more settled regions outside 20 au are still conducive to giant planet formation. This would naturally lead to giant planets forming at large radii, such as those that are leaving imprints in dust and gas in many older protoplanetary disks. If the vertically extended dust is a natural consequence of the dust evolution in a drift-dominated disk, as the VSI predicts, then it would be expected that all giant planets, including Jupiter, formed their core at radii >20 au.

A.D.B. and E.A.B. acknowledge support from NSF grant No. 1907653 and NASA grant No. XRP 80NSSC20K0259. J.A. acknowledges a Swedish Research Council grant (grant No. 2018-04867; PI: A. Johansen). M.L. acknowledges funding from the European Research Council (ERC Starting grant No. 101041466-EXODOSS).

Appendix A
Thermochemical Model

To predict the CO isotopologue emission we used the thermochemical code DALI (Bruderer et al. 2012; Bruderer 2013). This code allows us to take the physical conditions from the dynamical models, as well as stellar parameters, and calculate temperature and chemical abundance over the 2D model. We can then ray-trace the temperature and abundance structure to calculate the emission. The input stellar spectrum used is a stellar model with added UV (Zhang et al. 2021). The disk structure is based on the IM Lup structure of Zhang et al. (2021), and the disk parameters are given in Table 1.

For the dust optical properties we use the small (0.005–1 μm) and large (0.005–1000 μm) populations from Zhang et al. (2021; see also Birnstiel et al. 2018). The elemental abundances used in our model are shown in Table. 2. Contrary to Zhang et al. (2021), we assume a constant CO depletion factor of 100, the value measured at 100–150 au. To make a proper comparison with the data (Law et al. 2021), the image cubes from DALI are postprocessed. The individual channels in the cube are convolved with a circular Gaussian with a FWHM of 0.″15, before the channels are summed and an integrated intensity map is made. From this map a radial profile is extracted using a 30° wedge around the semimajor axes of the disk.

We ray-traced the $J = 2$–1 transitions of ^{13}CO and C^{18}O. The C^{18}O traces the deepest into the disk of these three lines and is thus the most sensitive to dust in the inner disk (see Figure 2). ^{13}CO traces higher up near the disk surface. These radial profiles are shown in Figure 6. While the ^{13}CO is overpredicted by the model, the behavior of the ^{13}CO still mirrors that of the C^{18}O, in the fact that, for the models with >450 $M_\oplus$ within 20–30 au, a dip in the emission profile can be seen. As such, the ^{13}CO emission supports our finding out of the C^{18}O emission.

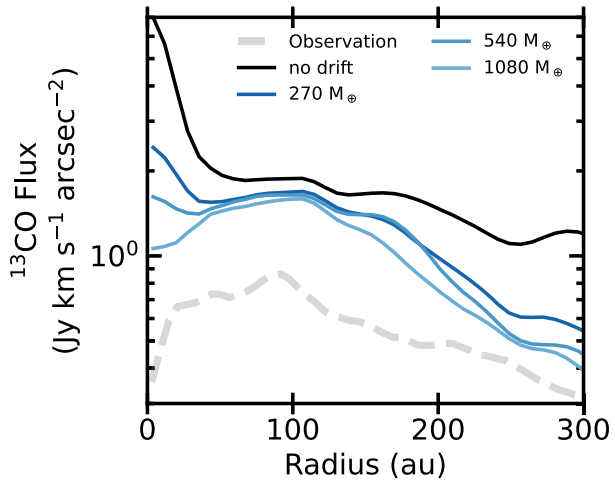

Figure 6. Same as Figure 2 but for ^{13}CO instead of C^{18}O. Again, >540 $M_\oplus$ is required to create an inner-disk depression.

Table 1
Thermochemical Modeling Parameters

Parameter	Value	Explanation
$M_\star$	1.1 $M_\odot$	Stellar mass
$L_\star$	2.57 $L_\odot$	Stellar luminosity
$M_{\rm gas}$	0.2 $M_\odot$	Disk gas mass
$M_{\rm dust,large}$	0.002 $M_\odot$	Large dust mass
$M_{\rm dust,small}$	2×10^{-4} $M_\odot$	Small dust mass
$R_{\rm crit}$	100 au	Critical radius
Σ_c	28.4 g cm^{-2}	Gas surface density at R_c
γ	1	Gas surface density slope
h_c	0.1	Gas scale height at critical radius
ψ	0.17	Flaring angle

Table 2
Elemental Abundances w.r.t Hydrogen

Element	Abundance w.r.t. H
H	1.0
He	7.59×10^{-2}
C	1.35×10^{-6}
N	2.14×10^{-5}
O	2.88×10^{-6}
Mg	4.17×10^{-9}
Si	7.94×10^{-8}
S	1.91×10^{-8}
Fe	4.27×10^{-9}

Appendix B
Dust Evolution Model

We ran a disk evolution model similar to Appelgren et al. (2020), which includes disk formation, viscous evolution, and the radial drift of dust, assuming different dust sizes. The

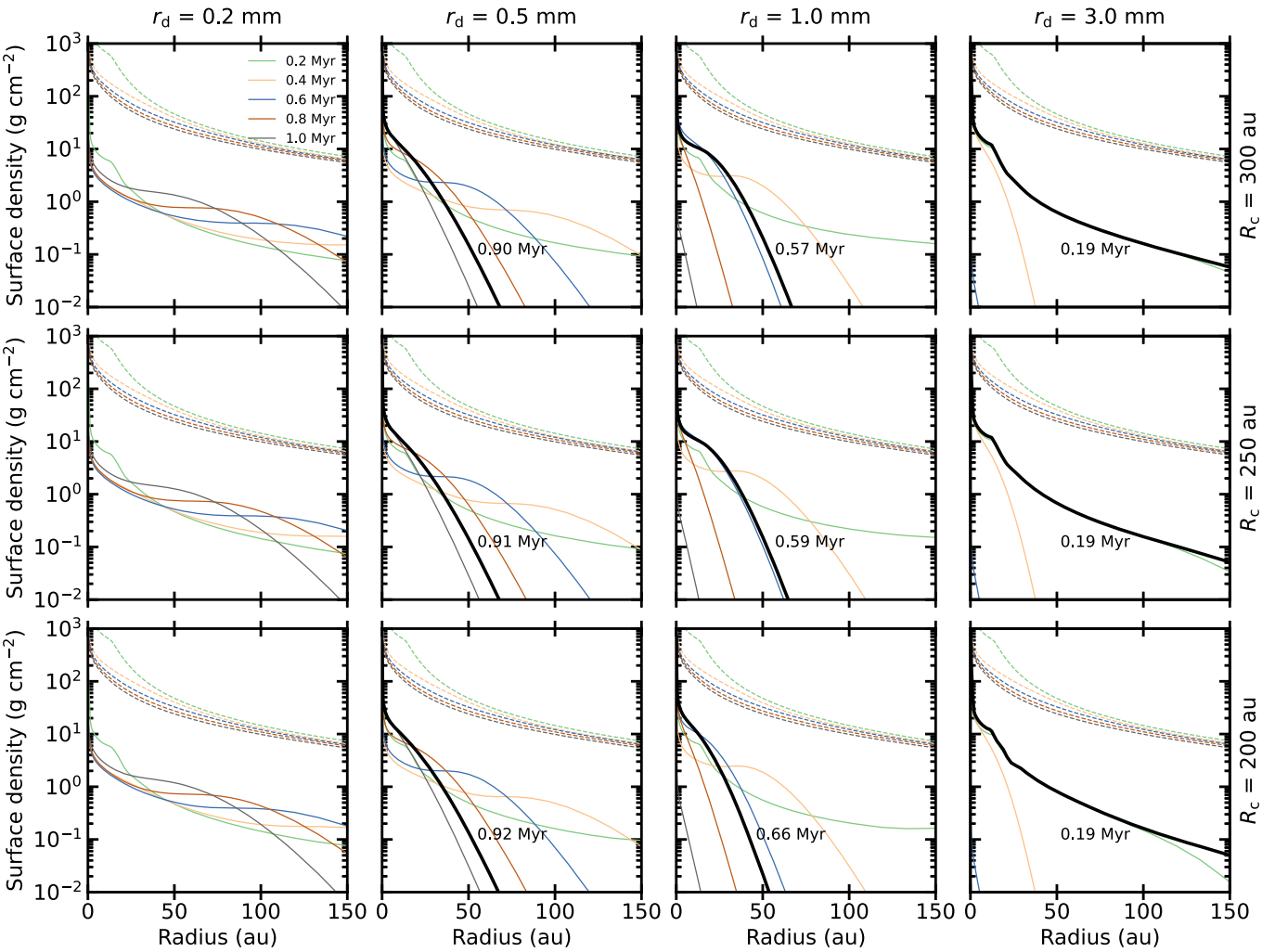

Figure 7. The evolution of the gas (dashed) and dust (solid) surface density for a selection of models from the grid of parameters explored. Each panel shows a combination of particle size and centrifugal radius. All models shown here used an initial dust-to-gas ratio of $Z = 0.01$. The black lines indicate the time, as labeled, at which 500 $M_\oplus$ have piled up inside 20 au. The model selected as the best fit for IM Lup is shown in the center-right panel, with a particle size of 1 mm and a centrifugal radius of 250 au. Changing the centrifugal radius has a minor effect on the evolution of the dust, but it affects the size of the gas disk at the time of the pileup. Models with particle sizes of 3 mm only reach 500 $M_\oplus$ of dust within 20 au just after the disk has finished forming, and would thus likely represent objects that are still embedded in their natal envelope. In the models with dust particles that are 0.2 mm in size, dust drift is too inefficient to pile up 500 $M_\oplus$ in the inner 20 au at any time.

formation of the disk is modeled starting from the gravitational collapse of an overdense Bonnor–Ebert sphere (Bonnor 1956; Ebert 1957). During disk formation the largest radius at which material lands on the disk is the maximum centrifugal radius, given by the following equation:

$$R_c = \frac{\Omega_0^2 r_{cf}(t)^4}{GM(r_{cf})}. \quad \text{(B1)}$$

Here, Ω_0 is the solid rotation rate of the cloud core, r_{cf} is the radius of the outwards-expanding collapse front, and $M(r_{cf})$ is the total mass inside the collapse front radius. For a molecular cloud core of a given mass, changing the centrifugal radius effectively sets its angular momentum. Different values for R_c therefore result in different disk sizes and masses.

The speed at which dust particles drift depends on their Stokes numbers, with a maximum drift rate at a Stokes number around unity. In the Epstein drag regime the Stokes number is set by the following equation:

$$\tau_s = \frac{\sqrt{2\pi}\rho_d a_d}{\Sigma_g}, \quad \text{(B2)}$$

where ρ_d is the material density of the dust particles, a_p is the size of the dust particles, and Σ_g is the gas surface density.

The mass of the dust disk is determined not only by the mass and angular momentum of the cloud core but also by the assumed dust-to-gas ratio of the cloud core. We will keep the dust-to-gas ratio fixed to the nominal ISM value of $Z = 0.01$.

We ran the disk evolution model for a grid of centrifugal radii and dust sizes. The gas disk in IM Lup extends out to 1200 au (Zhang et al. 2021). Because of the large size of the gas disk, the grid of centrifugal radii ranged from 150 to 300 au in steps of 50 au. These large values of the centrifugal radius, together with a viscous α parameter of $\alpha_\nu = 10^{-2}$, ensures that the gas disks are able to expand out to about 1000 au within

1 Myr, which is the estimated age of IM Lup. We ran the model with fixed particle sizes of 0.1, 0.2, 0.5, 1, and 3 mm.

From this grid of models, the case which best fits IM Lup had a centrifugal radius of 250 au, and 1 mm sized dust grains. The age of this disk when it best matched IM Lup was 0.59 Myr. This selection was based on the model piling up sufficient dust ($\sim$500 $M_\oplus$) within the inner 20 au (Bosman et al. 2021; Sierra et al. 2021), while having a gas radius which extends to about 1000 au and an age of about 1 Myr or less when this pileup occurs.

To explore the dependency of our preferred model to key parameters we explored variations on the total mass of solids and the radial extent of the inner-disk dust pileup. The resulting surface densities are shown in Figure 7. The choice of centrifugal radius has a very minor effect on the disk evolution. A smaller centrifugal radius delays the dust pileup very slightly. Particles sizes smaller than 0.5 mm do not lead to a significant pileup in the inner disk within 1 Myr (Figure 7, column 1). An increased particle size results in earlier pileups, such that for the 3 mm sized dust the pileup occurs just when the disk has finished forming. These disks would represent objects still embedded in their natal envelope and are therefore rejected. Models with 0.5 or 1 mm sized dust display similar pileups, but the 0.5 mm models pile up about 0.3 Myr later.

We finally verify that the gas accretion rate onto the host star, regulated by the disk mass and chosen α_ν value, is consistent with the young age of IM Lup. The nominal disk results in a sufficiently high accretion rate of $1.2 \times 10^{-7} M_\odot\,\mathrm{yr}^{-1}$, which, given uncertainties, moderately exceeds the inferred values in IM Lup of $\sim 10^{-8} M_\odot\,\mathrm{yr}^{-1}$ (Alcalá et al. 2017).

Appendix C
Vertical Shear Instability

In this appendix we explore how the radial range of the VSI-prone region depends on various model assumptions, with the aim to demonstrate that in a plausible parameter regime the VSI could be an explanation for the high particle scale heights inferred in the inner disk of IM Lup. We directly follow here the work of Lin & Youdin (2015).

As discussed in the main text, our results strongly depend on the assumed dust opacity. We therefore show our cooling time results for different Rosseland mean dust opacities, with a temperature dependency following Bell & Lin (1994) and an ISM-like dust size distribution, i.e., MRN (Savvidou et al. 2020). Then, by reducing or increasing the opacity by a factor of 2, we illustrate the trend when considering, respectively, subsolar or supersolar mass fractions of sub-10 μm grains. The opacity dependency of the cooling times as a function of orbital radius can be seen in Figure 9. An important caveat is that the dust distribution and resulting opacities are not well constrained for IM Lup, and may also be different in the inner and outer disk. A further exploration of the effects of the dust growth and disk evolution can be found in Fukuhara et al. (2021), who find the VSI suppressed in subsolar dust-to-gas environments. Future work could thus aim to link the opacity to a modeled particle size distribution and local dust-to-gas ratio.

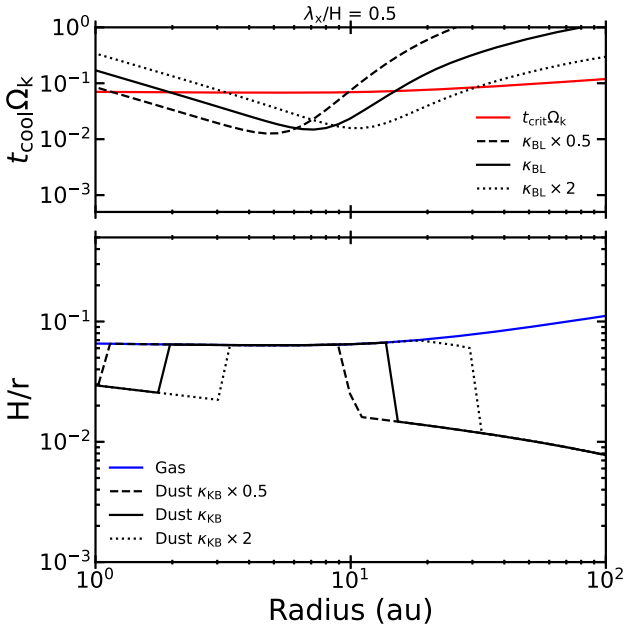

Figure 8. Same as Figure 4, but assuming a wavelength mode of $\lambda_x = 0.5\ H_g$. At longer wavelengths cooling is less efficient in the optically thick regions of the disk. As a result, the inner edge of the VSI-active region moves outwards and millimeter-sized dust particles remain settled in the innermost region of the disk.

In the inner, optically thick part of the disk, the cooling time depends on the length scale of the fastest-growing VSI mode. We explore different values, with modes between $\lambda_x/H = 0.05$, 0.5, and 1, in Figure 9, in line with the typical parameter range explored in VSI studies $\lambda_x/H \sim \mathcal{O}(0.5)$ (e.g., Pfeil & Klahr 2019). For the largest-scale VSI modes, comparable to the gas scale height, we find the VSI to be nearly fully suppressed, with the exception of a small region around 10 au. We also illustrate how the VSI region with high particle scale height is reduced for the $\lambda_x/H = 0.5$ case (Figure 8), compared to the $\lambda_x/H = 0.1$ case in the main text (Figure 4). Figure 8 illustrates that the inner edge of the VSI region is now located within the inner few astronomical units of the disk. Such a close-in inner VSI edge in the particle scale height would not be observable with the CO observations presented here.

In practice, it is not clear how to determine the fastest-growing VSI mode for the IM Lup disk model, as other sources of turbulence could dampen small-scale modes. Lin & Youdin (2015) provide a heuristic argument to determine a minimal growth scale by requiring the growth rate to exceed the viscous timescale $t_{\rm visc} \approx \lambda^2/\alpha_{\rm damp} c_s H$ on that scale. However, the appropriate value for $\alpha_{\rm damp}$ remains uncertain, as $\alpha_{\rm damp}$ is not necessarily equal to the vertical particle α_z or the ad hoc α_ν to evolve the disk in time (Appendix B). Indeed, simulations of VSI turbulence with the streaming instability (Schäfer & Johansen 2022) or disk turbulence under nonideal MHD conditions (Cui & Bai 2020) show a complex interplay. With these caveats in mind, Figure 9 shows results for a viscous cutoff with $\alpha_{\rm damp} = 10^{-4}$ and $\alpha_{\rm damp} = 10^{-3}$ (dashed lines). Larger vales of $\alpha_{\rm damp}$ would drive scales toward the local gas scale height and suppress the VSI on global scales.

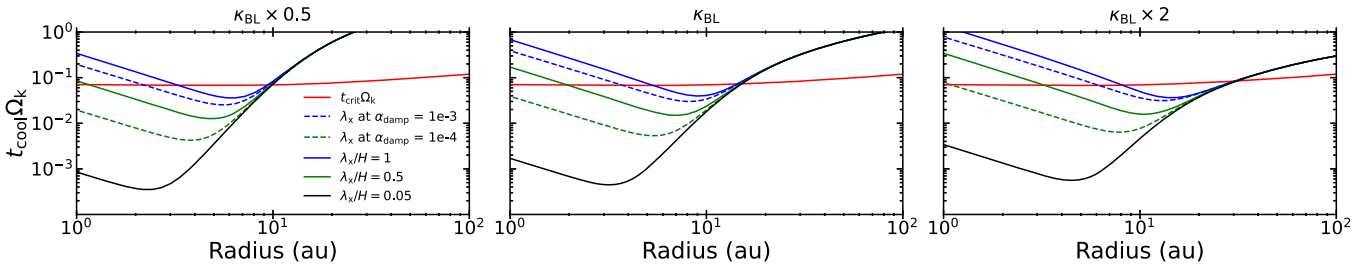

Figure 9. The effect of Rosseland mean opacity (κ_{BL}) and VSI wavelength mode (λ_x) on the dimensionless cooling-time parameter $t_{cool}\Omega_k$. At cooling times below $t_{crit}\Omega_k$ the VSI can become active. An increased opacity increases the cooling time in the inner, optically thick regions of the disk and decreases the cooling time in the outer, optically thin disk regions. As a result the VSI-prone region shifts outwards in the disk.

ORCID iDs

Arthur D. Bosman https://orcid.org/0000-0003-4001-3589
Johan Appelgren https://orcid.org/0000-0001-6168-1792
Edwin A. Bergin https://orcid.org/0000-0003-4179-6394
Michiel Lambrechts https://orcid.org/0000-0001-9321-5198
Anders Johansen https://orcid.org/0000-0002-5893-6165

References

Alcalá, J. M., Manara, C. F., Natta, A., et al. 2017, A&A, 600, A20
Andrews, S. M., Huang, J., Pérez, L. M., et al. 2018, ApJL, 869, L41
Appelgren, J., Lambrechts, M., & Johansen, A. 2020, A&A, 638, A156
Banzatti, A., Pascucci, I., Bosman, A. D., et al. 2020, ApJ, 903, 124
Bell, K. R., & Lin, D. N. C. 1994, ApJ, 427, 987
Birnstiel, T., Dullemond, C. P., & Brauer, F. 2010, A&A, 513, A79
Birnstiel, T., Dullemond, C. P., Zhu, Z., et al. 2018, ApJL, 869, L45
Birnstiel, T., Klahr, H., & Ercolano, B. 2012, A&A, 539, A148
Bitsch, B., Izidoro, A., Johansen, A., et al. 2019, A&A, 623, A88
Bonnor, W. B. 1956, MNRAS, 116, 351
Bosman, A. D., Bergin, E. A., Calahan, J., & Duval, S. E. 2022, ApJL, 930, L26
Bosman, A. D., Bergin, E. A., Loomis, R. A., et al. 2021, ApJS, 257, 15
Bosman, A. D., Bruderer, S., & van Dishoeck, E. F. 2017, A&A, 601, A36
Bosman, A. D., Cridland, A. J., & Miguel, Y. 2019, A&A, 632, L11
Bruderer, S. 2013, A&A, 559, A46
Bruderer, S., van Dishoeck, E. F., Doty, S. D., & Herczeg, G. J. 2012, A&A, 541, A91
Carrera, D., Johansen, A., & Davies, M. B. 2015, A&A, 579, A43
Cleeves, L. I., Öberg, K. I., Wilner, D. J., et al. 2018, ApJ, 865, 155
Cui, C., & Bai, X.-N. 2020, ApJ, 891, 30
Cuzzi, J. N., & Zahnle, K. J. 2004, ApJ, 614, 490
Drazkowska, J., Bitsch, B., Lambrechts, M., et al. 2022, arXiv:2203.09759
Dullemond, C. P., Birnstiel, T., Huang, J., et al. 2018, ApJL, 869, L46
Ebert, R. 1957, ZA, 42, 263
Flock, M., Nelson, R. P., Turner, N. J., et al. 2017, ApJ, 850, 131
Fukuhara, Y., Okuzumi, S., & Ono, T. 2021, ApJ, 914, 132
Haisch, K. E. J., Lada, E. A., & Lada, C. J. 2001, ApJL, 553, L153
Harsono, D., Persson, M. V., Ramos, A., et al. 2020, A&A, 636, A26
Hu, X., Li, Z.-Y., Zhu, Z., & Yang, C.-C. 2022, MNRAS, 516, 2006
Huang, J., Andrews, S. M., Dullemond, C. P., et al. 2018, ApJL, 869, L42
Johansen, A., & Bitsch, B. 2019, A&A, 631, A70
Johansen, A., Blum, J., Tanaka, H., et al. 2014, in Protostars and Planets VI, ed. H. Beuther et al. (Tucson, AZ: Univ. Arizona Press), 547
Johansen, A., & Lambrechts, M. 2017, AREPS, 45, 359
Lambrechts, M., & Johansen, A. 2012, A&A, 544, A32
Lambrechts, M., & Johansen, A. 2014, A&A, 572, A107
Law, C. J., Loomis, R. A., Teague, R., et al. 2021, ApJS, 257, 3
Li, R., & Youdin, A. N. 2021, ApJ, 919, 107
Lin, M.-K., & Youdin, A. N. 2015, ApJ, 811, 17
Mawet, D., Absil, O., Montagnier, G., et al. 2012, A&A, 544, A131
Mulders, G. D., Pascucci, I., Ciesla, F. J., & Fernandes, R. B. 2021, ApJ, 920, 66
Nelson, R. P., Gressel, O., & Umurhan, O. M. 2013, MNRAS, 435, 2610
Öberg, K. I., & Wordsworth, R. 2019, AJ, 158, 194
Ormel, C. W. 2017, in Astrophysics and Space Science Library, Formation, Evolution, and Dynamics of Young Solar Systems, ed. M. Pessah & O. Gressel, Vol. 445 (Berlin: Springer), 197
Pfeil, T., & Klahr, H. 2019, ApJ, 871, 150
Pinte, C., Dent, W. R. F., Ménard, F., et al. 2016, ApJ, 816, 25
Pinte, C., & Laibe, G. 2014, A&A, 565, A129
Pinte, C., Price, D. J., Ménard, F., et al. 2020, ApJL, 890, L9
Pinte, C., Teague, R., Flaherty, K., et al. 2022, arXiv:2203.09528
Pollack, J. B., Hubickyj, O., Bodenheimer, P., et al. 1996, Icar, 124, 62
Rabago, I., & Zhu, Z. 2021, MNRAS, 502, 5325
Riols, A., & Lesur, G. 2018, A&A, 617, A117
Salyk, C., Pontoppidan, K. M., Blake, G. A., Najita, J. R., & Carr, J. S. 2011, ApJ, 731, 130
Savvidou, S., Bitsch, B., & Lambrechts, M. 2020, A&A, 640, A63
Schäfer, U., & Johansen, A. 2022, A&A, 666, A98
Sierra, A., Pérez, L. M., Zhang, K., et al. 2021, ApJS, 257, 14
Teague, R., Bae, J., & Bergin, E. A. 2019, Natur, 574, 378
Toomre, A. 1964, ApJ, 139, 1217
Trapman, L., Facchini, S., Hogerheijde, M. R., van Dishoeck, E. F., & Bruderer, S. 2019, A&A, 629, A79
Urpin, V., & Brandenburg, A. 1998, MNRAS, 294, 399
Verrios, H. J., Price, D. J., Pinte, C., Hilder, T., & Calcino, J. 2022, ApJL, 934, L11
Villenave, M., Stapelfeldt, K. R., Duchêne, G., et al. 2022, ApJ, 930, 11
Weidenschilling, S. J. 1977, MNRAS, 180, 57
Yang, C.-C., Johansen, A., & Carrera, D. 2017, A&A, 606, A80
Yang, C.-C., Mac Low, M.-M., & Johansen, A. 2018, ApJ, 868, 27
Zhang, K., Booth, A. S., Law, C. J., et al. 2021, ApJS, 257, 5
Zhang, K., Schwarz, K. R., & Bergin, E. A. 2020, ApJL, 891, L17
Zhang, S., Zhu, Z., Huang, J., et al. 2018, ApJ, 869, L47